This article was downloaded by: [Renmin University of China]
On: 13 October 2013, At: 10:33
Publisher: Taylor & Francis
Informa Ltd Registered in England and Wales Registered Number: 1072954 Registered office: Mortimer House, 37-41 Mortimer Street, London W1T 3JH, UK

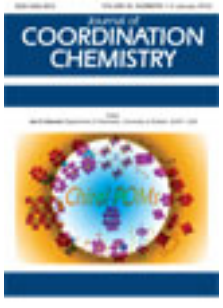

Journal of Coordination Chemistry
Publication details, including instructions for authors and subscription information:
http://www.tandfonline.com/loi/gcoo20

Prolonging luminescent lifetimes by introducing bis(maleonitriledithiolato)metalate anions with a fluorescent organic cation

Fang-Ming Wang [a b], Li-Zhuang Chen [b], Yang-Mei Liu [a], Chang-Sheng Lu [a], Xian-Ying Duan [a] & Qing-Jin Meng [a]

[a] State Key Laboratory of Coordination Chemistry, Nanjing National Laboratory of Microstructures, School of Chemistry and Chemical Engineering, Nanjing University, Nanjing 210023, P.R. China

[b] School of Biology and Chemical Engineering, Jiangsu University of Science and Technology, Zhenjiang 212003, P.R. China

Published online: 14 Dec 2011.

To cite this article: Fang-Ming Wang, Li-Zhuang Chen, Yang-Mei Liu, Chang-Sheng Lu, Xian-Ying Duan & Qing-Jin Meng (2012) Prolonging luminescent lifetimes by introducing bis(maleonitriledithiolato)metalate anions with a fluorescent organic cation, Journal of Coordination Chemistry, 65:1, 87-103, DOI: 10.1080/00958972.2011.641539

To link to this article: http://dx.doi.org/10.1080/00958972.2011.641539

PLEASE SCROLL DOWN FOR ARTICLE

Taylor & Francis makes every effort to ensure the accuracy of all the information (the "Content") contained in the publications on our platform. However, Taylor & Francis, our agents, and our licensors make no representations or warranties whatsoever as to the accuracy, completeness, or suitability for any purpose of the Content. Any opinions and views expressed in this publication are the opinions and views of the authors, and are not the views of or endorsed by Taylor & Francis. The accuracy of the Content should not be relied upon and should be independently verified with primary sources of information. Taylor and Francis shall not be liable for any losses, actions, claims, proceedings, demands, costs, expenses, damages, and other liabilities whatsoever or howsoever caused arising directly or indirectly in connection with, in relation to or arising out of the use of the Content.

This article may be used for research, teaching, and private study purposes. Any substantial or systematic reproduction, redistribution, reselling, loan, sub-licensing, systematic supply, or distribution in any form to anyone is expressly forbidden. Terms & Conditions of access and use can be found at http://www.tandfonline.com/page/terms-and-conditions

Downloaded by [Renmin University of China] at 10:33 13 October 2013

Journal of Coordination Chemistry
Vol. 65, No. 1, 10 January 2012, 87–103

Taylor & Francis
Taylor & Francis Group

Downloaded by [Renmin University of China] at 10:33 13 October 2013

Prolonging luminescent lifetimes by introducing bis(maleonitriledithiolato)metalate anions with a fluorescent organic cation

FANG-MING WANG*†‡, LI-ZHUANG CHEN‡, YANG-MEI LIU†, CHANG-SHENG LU†, XIAN-YING DUAN† and QING-JIN MENG*†

†State Key Laboratory of Coordination Chemistry, Nanjing National Laboratory of Microstructures, School of Chemistry and Chemical Engineering, Nanjing University, Nanjing 210023, P.R. China
‡School of Biology and Chemical Engineering, Jiangsu University of Science and Technology, Zhenjiang 212003, P.R. China

(*Received 10 August 2011; in final form 8 November 2011*)

A new organic fluorescent ionic compound [MOBIP]I (**1**) (MOBIP$^+$ = 1-methyl-2-oxo-3-(1*H*-benzimidazol-2(3*H*)-ylidene)-2,3-dihydropyridinium) was synthesized and used to prepare seven maleonitriledithiolate metal complexes $[MOBIP]_n[M(mnt)_2]$ by substitution of the iodide ion with $[M(mnt)_2]^{n-}$ (M = Cu^{2+} (**2**), Ni^{2+} (**3a**), Ni^{3+} (**3b**), Zn^{2+} (**4**), Cd^{2+} (**5**), Pd^{2+} (**6**), and Pt^{2+} (**7**)). An investigation of fluorescence properties shows that these complexes are a new series of solution luminescent complexes of maleonitriledithiolate derivatives with strong blue light fluorescence in daylight by irradiation with UV light with high quantum yields. They display similar symmetric emissions with λ_{em} at the deep blue region of ~426 nm upon excitation at ~364 nm in DMF, caused by **L**–**L** transition of MOBIP$^+$. Existence of $[M(mnt)_2]^{n-}$ anions in the solution prolongs the fluorescent lifetimes. For all these compounds in the solid state, the fluorescent emission is blue-shifted and more narrow than that in solution. Based on their crystal structure analysis, the weak stacking interactions in compounds cause the difference of their fluorescence spectrum. Investigations of variable-temperature magnetic susceptibility indicate that **2** has weak antiferromagnetic coupling, while **3b** exhibits stronger antiferromagnetic coupling.

Keywords: Bis(maleonitriledithiolato)metalate anion; Fluorescent properties; Crystal structure; Magnetic properties

1. Introduction

Recently, luminescent materials have provoked interest for their applications, such as light-emitting diodes, fluorescent sensors and probes, nonlinear optics, photoconductors, photovoltaics, upconversion lasing [1–9]. Research for luminescent materials focuses on higher quantum yields (Φ_f) of fluorescence emission, prolonging the complexes luminescence lifetime at room temperature, and wide emission bands ranging from UV to near infrared (NIR) [10, 11].

*Corresponding authors. Email: wangfmzj@yahoo.com.cn; mengqj@nju.edu.cn

ISSN 0095-8972 print/ISSN 1029-0389 online © 2012 Taylor & Francis
http://dx.doi.org/10.1080/00958972.2011.641539

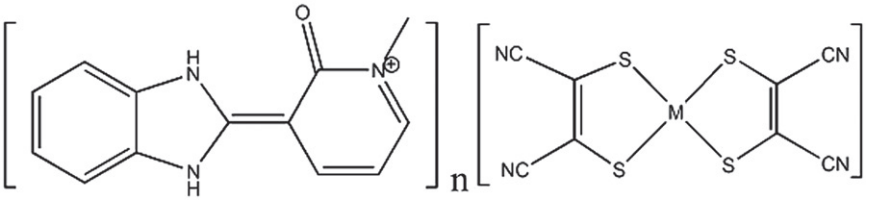

(n = 1 or 2; M = Cu^{2+}, Ni^{2+}, Ni^{3+}, Zn^{2+}, Cd^{2+}, Pd^{2+}, and Pt^{2+})

Scheme 1. Chemical formulae of the complexes.

Downloaded by [Renmin University of China] at 10:33 13 October 2013

Maleonitriledithiolate (mnt^{2-}) complexes of transition metals are useful building blocks for molecular conductors and magnets because they possess an extended electronically delocalized core [12–16], and they show variable properties affected by the intra- or inter-molecular contacts [17–20]. However, they are very rarely found in luminescent materials. Zuleta and coworkers reported the first series of solution luminescent complexes Pt(diimine)(mnt) in which the fluorescence of complexes were caused by **M–L** or **L–M** transitions [21]. Then Bremi *et al*. synthesized quasi-one-dimensional $[Pt(NH_2R)_4][Pt(mnt)_2]$ complexes in which the fluorescence was similar [22].

In this article, we have synthesized a new organic fluorescent ionic compound [MOBIP]I **(1)** ($MOBIP^+$ = 1-methyl-2-oxo-3-(1*H*-benzimidazol-2(3H)-ylidene)-2,3-dihydropyridinium) which displays strong blue emissions and high luminescence quantum efficiencies. In order to improve its luminescence, we prepared a new series of maleonitriledithiolate complexes by using $[M(mnt)_2]^{n-}$ anions to substitute for iodide (scheme 1). Herein we present the preparations, UV-Vis spectra, fluorescence, crystal structures, and magnetic susceptibilities of these compounds.

2. Experimental

2.1. *Chemicals and reagents*

All reagents of AR grade were used as supplied. The sodium salts of the ligand, *cis*-maleonitriledithiolate (Na_2mnt), were prepared according to the published method [23].

2.2. *Physical measurements*

Melting points were determined with an X-4 microscope melting-point testing apparatus (Shanghai). C, H, and N microanalyses were carried out with a Perkin-Elmer 240 elemental analyzer. Infrared (IR) spectra were recorded using KBr discs on a Bruker Vector 22 spectrophotometer from 4000 to 400 cm^{-1}. ^1H NMR spectra were obtained from a Bruker RX-500 spectrometer. Mass spectra were measured on a Finnigan LCQ^{TM} spectrometer. The UV-Vis-NIR spectra were recorded with a Shimadzu UV-3100 spectrophotometer. Fluorescence measurements were performed

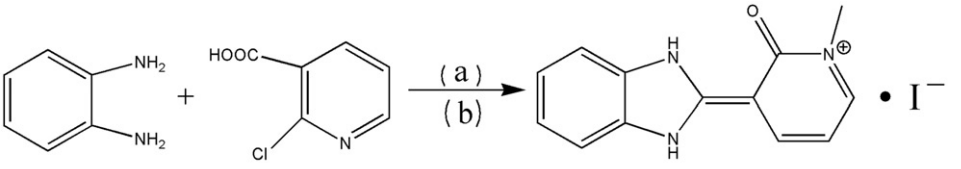

Reagents and conditions: (a) PPA, 170°C; (b) MeI in anhydrous acetone, reflux.

Scheme 2. Synthetic route of [MOBIP]I (**1**).

Downloaded by [Renmin University of China] at 10:33 13 October 2013

using a Perkin-Elmer LS 55 luminescence spectrometer with a 1 cm quartz cell at room temperature. Time resolved fluorescence spectra were performed using an Edinberge FLS920 luminescence spectrometer. Variable-temperature magnetic data for **2** and **3b** were obtained over the temperature range of 1.8–300 K using a Quantum Design MPMS-XL7 SQUID magnetometer.

2.3. *Synthesis of compounds*

2.3.1. Synthesis of [MOBIP]I (1). According to the literature method [24, 25], [MOBIP]I (**1**) was synthesized as shown in scheme 2. A mixture of 2-chloronicotinic acid (6.3 g, 40 mmol) and *o*-phenylenediamine (4.3 g, 40 mmol) in polyphosphoric acid was heated at 170°C for 8 h with stirring. The reaction mixture was then cooled to room temperature and poured into ice-water (200 mL). The solution pH was adjusted to 9.0 with ammonia. The pale-yellow precipitate was filtered and washed with water several times, and then dried *in vacuo*. Finally, the yellowish precipitate was dissolved in dry acetone (100 mL) by dropwise addition of a solution of methyl iodide (2.5 mL, 40 mmol) in dry acetone (10 mL) under an atmosphere of nitrogen. The reaction mixture was refluxed for 24 h. After cooling, the precipitate was filtered, washed with acetone, and then recrystallized in 80% ethanol solution. The yellowish micro-crystallite was collected and dried *in vacuo*. Yield: 7.6 g (54%). M.p.: 236°C. ^{1}H NMR (DMSO, 500 MHz) δ: 3.71 (s, 3 H, Me–H), 6.78 (m, 1 H, Py–H), 7.55 (dd, $J = 3.00$, 6.00 Hz, 2 H, Ph–H), 7.88 (dd, $J = 3.00$, 6.00 Hz, 2 H, Ph–H), 8.33 (d, $J = 6.50$ Hz, 1 H, Py–H), 8.60 (d, $J = 7.00$ Hz, 1 H, Py–H), 14.5 (br, 2 H, N–H); IR (KBr, cm^{-1}): 3388(s), 3126(m), 1647(s), 1624(m), 1572(s), 1451(w), 1414(w), 1345(w), 1286(m), 1233(w), 1180(w), 1135(w), 1044(w), 865(w), 768(m). MS (ESI): m/z 226.4 (M^+). Anal. Calcd for $C_{13}H_{12}IN_3O$ (%): C, 44.21; H, 3.42; N, 11.90. Found: C, 44.35; H, 3.28; N, 11.77.

2.3.2. Synthesis of [MOBIP]$_2$[Cu(mnt)$_2$] (2). A methanol solution of Na_2mnt (372 mg, 2.0 mmol) was mixed with a methanol solution of $CuCl_2 \cdot 2H_2O$ (171 mg, 1.0 mmol), stirred for 30 min at room temperature and filtered. A dark-red precipitate formed after adding dropwise a methanol solution containing [MOBIP]I (**1**) (704 mg, 2.0 mmol) to the filtrate, which was filtered off, washed with methanol, and then dried in vacuum. Yield: 622.1 mg (78.3%). Anal. Calcd for $C_{34}H_{24}CuN_{10}O_2S_4$ (%): C, 51.27; H, 3.04; N, 17.59. Found: C, 51.67; H, 2.63; N, 17.56. IR (KBr, cm^{-1}): ν(NH), 3420 m; ν(CN), 2196s; ν(C=C) of mnt^{2-}, 1460m. IR (KBr, cm^{-1}): 3420(m), 3155(m), 3121(m), 2196(s),

1657(s), 1623(m), 1572(s), 1460(m), 1393(w), 1347(w), 1290(m), 1244(w), 1193(w), 1150(w), 1112(w), 1032(w), 866(w), 766(m).

2.3.3. Synthesis of [MOBIP]$_2$[Ni(mnt)$_2$] (3a). This dark-brown complex was prepared by an analogous procedure replacing $CuCl_2 \cdot 2H_2O$ with $NiCl_2 \cdot 6H_2O$ (237 mg, 1.0 mmol). Yield: 659.3 mg (83.5%). Anal. Calcd for $C_{34}H_{24}NiN_{10}O_2S_4$ (%): C, 51.59; H, 3.06; N, 17.69. Found: C, 51.56; H, 2.75; N, 17.65. IR (KBr, cm^{-1}): ν(NH), 3419m; ν(CN), 2194s; ν(C=C) of mnt^{2-}, 1479m. 3419(m), 3180(m), 3126(m), 2194(s), 1656(s), 1623(m), 1573(s), 1479(m), 1392(w), 1347(w), 1291(m), 1244(w), 1194(w), 1151(w), 1109(w), 1035(w), 867(w), 763(m).

2.3.4. Synthesis of [MOBIP][Ni(mnt)$_2$] (3b). An acetonitrile solution (10 mL) of I_2 (88.5 mg, 0.35 mmol) was slowly added to an acetonitrile solution (20 mL) of **3a** (394.5 mg, 0.5 mmol) and the mixture was stirred for 12 h. Methanol (120 mL) was then added, and the mixture was allowed to stand overnight, black micro-crystals formed and were filtered off, then were washed with methanol, and dried in vacuum. Yield: 215.7 mg (76.3%). Anal. Calcd for $C_{21}H_{12}N_7NiOS_4$ (%): C, 44.62; H, 2.14; N, 17.34. Found: C, 44.56; H, 1.89; N, 17.45. IR (KBr, cm^{-1}): ν(NH), 3419m; ν(CN), 2210s; ν(C=C) of mnt^{2-}, 1455m. 3419(s), 3146(m), 3112(m), 2210(m), 1660(m), 1624(m), 1567(s), 1455(w), 1397(w), 1344(w), 1288(w), 1234(w), 1190(w), 1160(w), 1101(w), 1045(w), 838(w), 754(m).

2.3.5. Synthesis of [MOBIP]$_2$[Zn(mnt)$_2$] (4). This orange complex was prepared by an analogous procedure replacing $CuCl_2 \cdot 2H_2O$ with $ZnCl_2$ (136 mg, 1.0 mmol). Yield: 608.3 mg (76.4%). Anal. Calcd for $C_{34}H_{24}ZnN_{10}O_2S_4$ (%): C, 51.16; H, 3.03; N, 17.55. Found: C, 51.16; H, 2.73; N, 17.48. IR (KBr, cm^{-1}): ν(NH), 3418m; ν(CN), 2194s; ν(C=C) of mnt^{2-}, 1439m. 3418(m), 3145(m), 3109(m), 2194(s), 1644(m), 1623(m), 1572(s), 1439(m), 1344(w), 1286(m), 1236(w), 1192(w), 1148(w), 1112(w), 1040(w), 864(w), 763(m).

2.3.6. Synthesis of [MOBIP]$_2$[Cd(mnt)$_2$] (5). This orange complex was obtained in a similar manner by replacing $CuCl_2 \cdot 2H_2O$ with $Cd(NO_3)_2 \cdot 4H_2O$ (308 mg, 1.0 mmol). The procedure was similar to the previous ones. Yield: 605.2 mg (71.6%). Anal. Calcd for $C_{34}H_{24}CdN_{10}O_2S_4$ (%): C, 48.31; H, 2.86; N, 16.57. Found: C, 48.36; H, 2.55; N, 16.45. IR (KBr, cm^{-1}): ν(NH), 3426m; ν(CN), 2193s; ν(C=C) of mnt^{2-}, 1440m. 3426(m), 3195(m), 3107(m), 2193(s), 1644(m), 1621(m), 1567(s), 1440(m), 1343(w), 1284(m), 1230(w), 1192(w), 1147(m), 1115(m), 1036(w), 856(w), 763(m).

2.3.7. Synthesis of [MOBIP]$_2$[Pd(mnt)$_2$] (6). This wine complex was obtained in a similar manner by replacing $CuCl_2 \cdot 2H_2O$ with $PdCl_2$ (177 mg, 1.0 mmol). Yield: 476.7 mg (56.8%). Anal. Calcd for $C_{34}H_{24}PdN_{10}O_2S_4$ (%): C, 48.66; H, 2.88; N, 16.69. Found: C, 48.63; H, 2.73; N, 16.65. IR (KBr, cm^{-1}): ν(NH), 3422m; ν(CN), 2197s; ν(C=C) of mnt^{2-}, 1479m. 3422(m), 3157(m), 3120(m), 2197(s), 1656(m), 1623(m), 1573(s), 1479(m), 1393(w), 1346(w), 1291(m), 1243(w), 1192(w), 1146(w), 1108(w), 1036(w), 863(w), 763(m).

Downloaded by [Renmin University of China] at 10:33 13 October 2013

2.3.8. Synthesis of $[MOBIP]_2[Pt(mnt)_2]$ (7). This dark-yellow complex was obtained in a similar manner by replacing $CuCl_2 \cdot 2H_2O$ with K_2PtCl_4 (415 mg, 1.0 mmol). Yield: 753.6 mg (81.4%). Anal. Calcd for $C_{34}H_{24}PtN_{10}O_2S_4$ (%): C, 44.01; H, 2.61; N, 15.09. Found: C, 44.23; H, 2.45; N, 15.05. IR (KBr, cm^{-1}): ν(NH), 3416m; ν(CN), 2194m; ν(C=C) of mnt^{2-}, 1452m. 3416(s), 3149(m), 3107(m), 2362(w), 2194(w), 1655(m), 1621(m), 1570(s), 1452(m), 1394(w), 1344(w), 1288(w), 1236(w), 1193(w), 1151(w), 1107(w), 1040(w), 868(w), 757(m).

Single crystals suitable for X-ray structure analysis of **2**, **3a**, **3b**, and **6** were obtained by evaporating solutions of the complexes in acetonitrile at room temperature for 2 weeks; compound **1** was recrystallized in 80% ethanol solution.

2.4. *X-ray crystallography*

Crystallographic data were collected using a Bruker SMART APEX II CCD-based diffractometer with graphite-monochromatic Mo-Kα radiation ($\lambda = 0.71073$ Å) at 291(2)K. Data reductions and absorption corrections were performed with SAINT and SADABS software packages [26], respectively. Structures were solved by direct methods using the SHELXL-97 software package [27]. Non-hydrogen atoms were refined anisotropically using the full-matrix least-squares method on F^2. All hydrogen atoms were placed at calculated positions (C–H = 0.930 Å for benzene, 0.960 Å for methyl) and refined riding on the parent with $U(H) = 1.2U$eq (bonded C of both pyridyl and methyl group) and $U(H) = 1.5U$eq (bonded C of methyl group). Details of the crystallographic parameters, data collection, and refinements for **1**, **2**, **3a**, **3b**, and **6** are summarized in table 1.

3. Results and discussion

3.1. *Synthetic strategy*

Pyridyl-benzimidazole derivatives are representative ligands in coordination and metallosupramolecular chemistry which often show luminescent properties [8–11]. However, fluorescence of these ligands would quench when with N-alkyl reactions of the pyridyl ring, because the pair of electrons on nitrogen was fixed by the alkyl group, reducing the conjugation of the group and destroying its excited state.

In order to avoid this, we introduced chloride on the pyridyl ring by using 2-chloronicotinic acid; the *o*-chloride would be substituted by oxygen when reacted in inorganic acids [24], strengthening the conjugation between oxygen, pyridyl ring, and benzimidazole ring. This should avoid luminescence quench even with N-alkyl reaction of pyridyl. Based on this synthetic idea, we formed a new organic fluorescent compound **1** [MOBIP]I (1-methyl-2-oxo-3-(1*H*-benzimidazol-2(3H)-ylidene)-2,3-dihydropyridinium iodide). Compound **1** was characterized by elemental analysis, IR, MS, UV, fluorescence spectra, and X-ray structure analysis.

3.2. *IR spectra*

The IR spectra of all eight compounds are complicated. The broad band at 3000–3600 cm^{-1} and strong absorption around 1650 cm^{-1} may be ascribed to ν(N–H) and

Downloaded by [Renmin University of China] at 10:33 13 October 2013

Downloaded by [Renmin University of China] at 10:33 13 October 2013

Table 1. Crystallographic data for **1**, **2**, **3a**, **3b**, and **6**.

Complex	**1**	**2**	**3a**	**3b**	**6**
Empirical formula	$C_{13}H_{12}N_3OI \cdot H_2O$	$C_{34}H_{24}CuN_{10}O_2S_4$	$C_{34}H_{24}NiN_{10}O_2S_4$	$C_{21}H_{12}N_7NiOS_4$	$C_{34}H_{24}PdN_{10}O_2S_4$
Formula weight	371.17	796.46	791.60	565.33	839.33
Wavelength (Å)	0.71073	0.71073	0.71073	0.71073	0.71073
Crystal system	Monoclinic	Triclinic	Triclinic	Monoclinic	Triclinic
Space group	$P2_1$	P-1	P-1	$P2_1/n$	P-1
Unit cell dimensions (Å, °)					
a	10.058(2)	8.6315(16)	8.723(2)	14.610(3)	8.577(4)
b	5.7973(14)	8.7687(17)	8.747(2)	10.4149(19)	8.746(4)
c	11.975(3)	12.539(2)	12.336(3)	15.524(3)	12.655(6)
α	90.00	101.019(3)	96.504(4)	90.00	101.254(10)
β	92.075(4)	96.215(4)	100.252(5)	103.339(3)	95.836(10)
γ	90.00	110.539(3)	110.445(4)	90.00	110.074(9)
Volume (Å^3), Z	697.8(3), 2	856.3(3), 1	852.0(3), 1	2298.5(7), 4	859.7(7)
Calculated density (g cm^{-3})	1.767	1.544	1.543	1.634	1.621
Absorption coefficient (mm^{-1})	2.296	0.931	0.864	1.239	0.832
F(000)	364	407	406	1148	424
Crystal size (mm^3)	$0.35 \times 0.15 \times 0.10$	$0.35 \times 0.25 \times 0.20$	$0.35 \times 0.25 \times 0.15$	$0.30 \times 0.25 \times 0.20$	$0.35 \times 0.20 \times 0.15$
Max. and min. transmission	0.794/0.669	0.829/0.757	0.877/0.773	0.780/0.698	0.882/0.820
θ range for data collection (°)	2.6–21.9	2.5–28.2	2.6–25.8	1.7–26.0	2.6–21.4
Limiting indices	$-10 \le h \le 12$; $-7 \le k \le 7$; $-12 \le l \le 14$	$-5 \le h \le 10$; $-10 \le k \le 9$; $-15 \le l \le 13$	$-7 \le h \le 10$; $-10 \le k \le 10$; $-14 \le l \le 15$	$-18 \le h \le 15$; $-12 \le k \le 9$; $-19 \le l \le 19$	$-10 \le h \le 9$; $-8 \le k \le 10$; $-14 \le l \le 15$
Reflections collected	3739	3360	3340	4494	3370
Independent reflection	1515	2878	2521	3049	2279
(R_{int})	0.0271	0.063	0.0722	0.045	0.0304
Goodness-of-fit on F^2	0.991	1.002	0.996	1.000	1.008
R_1	0.0346, 0.0442	0.0420, 0.0463	0.0424, 0.0528	0.0398, 0.0604	0.0518, 0.0765
wR_2	0.0568, 0.0580	0.1145, 0.1181	0.0862, 0.0889	0.0633, 0.0661	0.0782, 0.0835
Largest difference peak and hole (e Å^{-3})	1.07 and −0.41	0.40 and −0.46	0.70 and −0.35	0.62 and −0.34	0.75 and −0.73

Table 2. UV-Vis spectra [ε $(\text{mol L}^{-1})^{-1}\,\text{cm}^{-1}$ 10^4)] and fluorescence spectra of the synthesized compounds ($5 \times 10^{-7}\,\text{mol L}^{-1}$ in DMF).

		Fluorescence				
	UV-Vis	Excitation	Emission	Stokes shift	Fluorescent quantum yield	Lifetime
Compound	(λ, nm)/ε	λ_{max} (nm)	λ_{max} (nm)	(nm)	Φ_f	τ (ns)
1	366 (4.20) 264 (17.40)	363.5 (518.4)	425.5 (518.9)	62.0	0.70	3.76
2	485 (0.85) 367 (8.74) 285 (3.78) 264 (17.65)	363.5 (827.6)	426.5 (827.8)	63.0	0.54	3.84
3a	481 (0.94) 367 (8.30) 320 (6.81) 264 (20.15)	363.0 (856.8)	426.0 (855.8)	63.0	0.62	3.81
3b	485 (0.81) 367 (4.45) 316 (5.58) 265 (19.22)	363.5 (442.4)	425.5 (442.3)	62.0	0.56	3.80
4	485 (0.24) 367 (9.14) 265 (16.95)	365.0 (799.1)	425.5 (799.8)	60.5	0.49	3.75
5	485 (0.43) 368 (8.56) 264 (18.80)	364.0 (678.3)	425.5 (678.2)	61.5	0.45	3.87
6	444 (1.17) 367 (7.13) 287 (7.83) 265 (21.22)	361.5 (898.1)	424.5 (898.4)	63.0	0.62	3.77
7	485 (0.55) 367 (8.40) 285 (1.75) 265 (14.12)	364.5 (903.1)	426.0 (903.9)	61.5	0.67	3.92

Downloaded by [Renmin University of China] at 10:33 13 October 2013

ν(C=O) of $[\text{MOBIP}]^+$. Absorptions at ~2194 (2210 in **3b**), 1439–1479, and 1147–1160 cm^{-1} correspond to ν(C≡N), ν(C=C), and ν(C–S) of mnt^{2-}, respectively. Stretching of CN groups, i.e., ν(C≡N), is related to the charge (−1 to −3) on $[\text{M(mnt)}_2]^{n-}$ [28]. Comparing the ν(C≡N) of these complexes with those in references, it can be concluded that **2**, **3a**, **4**, **5**, **6**, and **7** have charge of −2, while **3b** has charge of −1.

3.3. *UV-Vis absorption and fluorescence spectroscopy*

UV-Vis absorption spectra of all seven complexes and [MOBIP]I (**1**) were measured in DMF from 250 to 700 nm, table 2. These compounds show similar absorptions. Absorptions at ~285 and 265 nm are due to **L**(π)–**L**(π*) transitions. According to the molecular structure of MOBIP^+, absorptions at ~367 nm should belong to **L**(n)–**L**(π*)

transition caused by the C=O [29]; bands at ~485 nm are assigned to MLCT absorptions for the metal dithiolene [30]. According to the reference and UV-Vis absorption spectra, the electronic transition of these compounds should be induced by n–π^* excited states.

Remarkably, these eight compounds emit strong blue light fluorescence in daylight by irradiation with UV light when dissolved in DMF at room temperature. These seven complexes in DMF are solution luminescent. All fluorescence data of these compounds at 5×10^{-7} mol L^{-1} in DMF are also shown in table 2. Emissions were measured between 380 and 600 nm *versus* excitations performed between 300 and 400 nm. The fluorescence quantum yields (ϕ_f) were measured as compared with quinine sulfate in order to evaluate their fluorescence [31].

The fluorescent data in table 2 show that all the compounds in DMF display similar symmetric emissions with λ_{em} at the deep blue region, ~426 nm, upon excitation at ~364 nm in DMF, with Stokes shifts of about 62 nm. Because mnt^{2-} itself is not photo-emitting, it is unlikely that emission is due to a **d**–**d** transition or **L**–**L** transition of anions [22], so fluorescence is caused by **L**–**L** transition of $MOBIP^+$. This transition mode is different from **LMCT** or **MLCT** modes of other solution luminescent maleonitriledithiolate complexes [21, 22].

ϕ_f of these eight compounds were high at 0.45–0.70 (table 2). Surprisingly, introduction of $[M(mnt)_2]^{n-}$ with $MOBIP^+$ prolongs the fluorescent lifetimes. The maximum value of fluorescent lifetime in complexes is 3.92 ns, 0.16 ns longer than the fluorescent lifetime of [MOBIP]I (**1**).

For solution luminescent complexes, the main factors which influence luminescence ability are transition modes, photon transfer efficiency, solvent effect, and steric effects [21, 32]. The luminescent differences between these seven complexes should be mainly caused by different spatial obstacles influence on the photon transfer induced by $[M(mnt)_2]^{n-}$ anions, because they have same transition mode and solvent effect.

As shown in table 2, the fluorescence intensity decreases in the order, $Ni^{2+} > Cu^{2+} > Zn^{2+} > Cd^{2+}$, in contrast with the order reported [33]. Probably, collisional quenching differences between the four complexes may be related to the structure of the complexes. The Zn^{2+} and Cd^{2+} complexes have tetrahedron configuration, while Ni^{2+} and Cu^{2+} complexes are square-planar geometry. Due to this, the collisional quenching caused by anions of Zn^{2+} and Cd^{2+} complexes is larger than for Ni^{2+} and Cu^{2+}. For anions with similar configuration, the collisional quenching will become larger, corresponding to the metal ionic radius increasing. However, these $[M(mnt)_2]^{n-}$ can prolong the fluorescent lifetimes because of their influence on photon transfer efficiency, enhanced by increasing the planarity of anions.

As to d^8 complexes (Ni^{2+}, Pd^{2+} and Pt^{2+}), their complexes have square-planar geometry [21]. With the metal ionic radius increasing, the photon transfer can be easier and collisional quenching to luminescence decreased. So the fluorescence intensity of d^8 complexes follows the order $Pt^{2+} > Pd^{2+} > Ni^{2+}$; the fluorescent lifetime of **7** is the longest one in all compounds.

When the stoichiometric ratio of cations and anions in **3a** and **3b** changed from 2 : 1 to 1 : 1, ϕ_f declined only 8.9%. Due to its higher nuclear charge, smaller ionic radius and more planarity, quenching by Ni^{3+} was lower than by Ni^{2+} [34].

When all these compounds are in the solid state, **1** exhibits a strong blue emission with $\lambda_{max} = 393$ nm with excitation at 357 nm at room temperature, while emissions of **2**–**7** are quenched. There exist a variety of molecular interactions which can result in

Downloaded by [Renmin University of China] at 10:33 13 October 2013

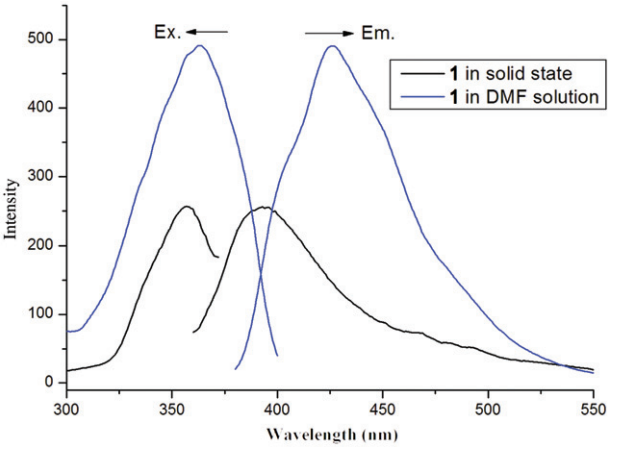

Figure 1. Excitation and emission spectra of **1** in the solid state and in DMF at room temperature (5×10^{-7} mol L^{-1}).

quenching, such as excited-state reactions, molecular rearrangement, energy transfer, ground state complex formation, and collisional quenching [34].

As shown in figure 1, Stokes shift of **1** is 36 nm in the solid state, nearly half the value in DMF solution. Compared with the fluorescent emission of **1**, the emission in the solid state is blue-shifted and more narrow than that in solution. This phenomenon is attributable to the absence of intermolecular interactions in solution, most likely π–π stacking interactions [35].

In order to study how molecular interactions influence fluorescence in the solid compounds, we obtained single crystals of **1**, **2**, **3a**, **3b**, and **6**.

3.4. *Crystal structures*

3.4.1. X-ray structures of 1. Crystal analysis reveals that **1** crystallizes in the monoclinic space group $P2_1$; selected bond lengths and angles are listed in table S1.

As shown in figure 2(a), one MOBIP$^+$ balanced with an iodide in an asymmetric unit as well as one water molecule. MOBIP$^+$ has bond lengths between C3–C7 and C2–C3 of 1.438(6) Å and 1.439(7) Å, which means there exist super-conjugation and electron delocalization between the carbonyl group and C=C bonds. There also exist strong intramolecular H-bonding interactions between O1 and neighboring N2 in the cation (with H-bonding parameters of $d_{N\cdots O} = 2.695(5)$ Å and $\angle N\text{–}H\cdots O = 121(2)^\circ$), which bind O1, C2, C3, C7, and N2 to a six-member ring. The dihedral angle between the benzimidazole plane and pyridyl plane is 2.769(124)°. These structural characters enhance the molecular coplanarity and luminescence capability of this organic cation.

The packing diagram and intermolecular H-bonding of **1** viewed along the *a*-axis are shown in figure 2(b). BMOIP$^+$ are stacked into two crossing columns with crossing angle between the columns of 73.893(50)°. Within the cation columns, the cations slipped, presenting strong $\pi\cdots\pi$ interactions which induced the fluorescent emissions of **1** in the solid state to become blue-shifted and narrow. The centroid-to-centroid

Downloaded by [Renmin University of China] at 10:33 13 October 2013

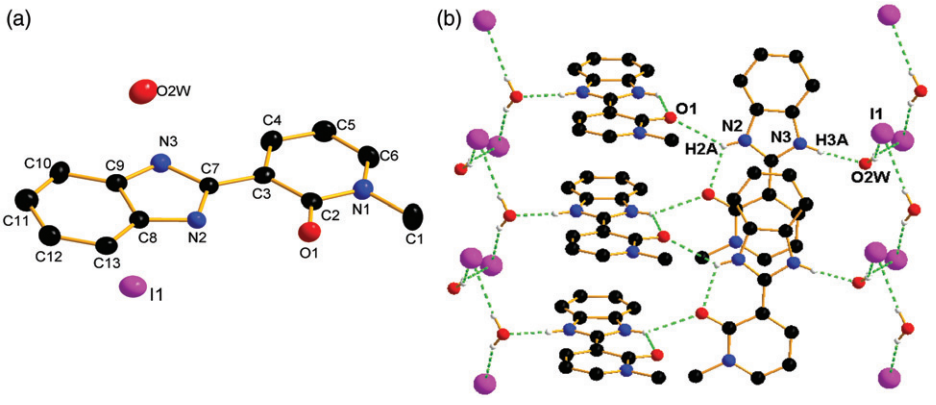

Figure 2. (a) ORTEP view of **1** with atom labeling and (b) the H-bonding interactions in layers of **1** are viewed along the *a*-axis.

distance between benzimidazole and pyridine ring is 3.5497(5) Å (figure S1). Two neighboring columns are bonded by intermolecular H-bonding interactions between N2 of imidazoline ring and O1 of pyridyl (with H-bonding parameters of $d_{N\cdots O} = 3.118(5)$ Å and $\angle N\text{–}H\cdots O = 135.5°$).

Among every two crossing cation columns, there exist 1-D zigzag chains from two intermolecular H-bonding interactions between the iodide and H_2O (with H-bonding parameters of $d_{O\cdots I} = 3.476(4)$ Å and $\angle O\text{–}H\cdots I = 165.8°$, $d_{O\cdots I} = 3.444(4)$ Å and $\angle O\text{–}H\cdots I = 159.7°$, respectively). Between the 1-D chains and the cation columns, there exists an intermolecular H-bond between O2W and N3 from imidazoline of cation (with H-bonding parameters of $d_{N\cdots O} = 2.680(5)$ Å and $\angle N\text{–}H\cdots O = 173.7°$).

3.4.2. X-ray structures of 2, 3a, 3b, and 6. Crystal analyses reveal that **2**, **3a**, and **6** are isostructural with very similar packing structures. Selected bond lengths and angles for **2**, **3a**, and **6** are listed in table 3. As shown in figure 3(a), there is one half of an anion with one cation in an asymmetric unit; the metal is located on a crystallographic inversion center, which imposes perfect planarity to the four coordinated S-atoms with the metal. The Cu–S bond lengths range from 2.2536(7) to 2.2791(7) Å, the bite angle in the chelating ring of S–Cu–S is 90.64(2)° in **2**; bond lengths of Ni–S range from 2.1598(8) to 2.1681(8) Å, the bite angle in the chelating ring of S–Ni–S is 91.93(3)° in **3a**; bond lengths of Pd–S range from 2.2762(14) to 2.2909(14) Å, the bite angle in the chelating ring of S–Pd–S is 90.30(5)° in **6** (table 3). These bonding parameters are comparable with those values in reported $[Cu(mnt)_2]^{2-}$, $[Ni(mnt)_2]^{2-}$, or $[Pd(mnt)_2]^{2-}$ complexes [36, 37]. A striking feature of the structure for these three complexes is that $[M(mnt)_2]^{2-}$ exhibits Z-shaped nonplanar geometry with the ligand fragment bent away from the MS_4 plane with a dihedral angle of 13.6° in **2** (10.2° in **3** and 9.5° in **6** (figure 3b). The most favorable structures of $[Cu(mnt)_2]^{2-}$, $[Ni(mnt)_2]^{2-}$, and $[Pd(mnt)_2]^{2-}$ are planar, and nonplanar geometry is rare.

Crystals **2**, **3a**, and **6** were packed layer-by-layer (figure 4a). Within layers, two types of H-bonding interactions are observed. The intermolecular H-bonding interaction is between the imidazoline of the cations and the nitrile of the anions (with H-bonding

Downloaded by [Renmin University of China] at 10:33 13 October 2013

Downloaded by [Renmin University of China] at 10:33 13 October 2013

Table 3. Selected bond lengths (Å) and angles (°) in complexes.

Complex **2**			
Cu(1)–S(1)	2.2791(7)	S(1A)–Cu(1)–S(1)	180.000(19)
Cu(1)–S(2)	2.2536(7)	S(2A)–Cu(1)–S(2)	180.0
S(2)–Cu(1)–S(1)	90.64(2)	C(16)–S(1)–Cu(1)	100.69(8)
S(2)–Cu(1)–S(1A)	89.36(2)	C(14)–S(2)–Cu(1)	101.24(8)
Complex **3a**			
Ni(1)–S(1)	2.1598(8)	S(2)–Ni(1)–S(2A)	180.000(1)
Ni(1)–S(2)	2.1681(8)	S(1A)–Ni(1)–S(1)	180.0
S(1)–Ni(1)–S(2)	91.93(3)	C(14)–S(1)–Ni(1)	103.00(9)
S(1)–Ni(1)–S(2A)	88.07(3)	C(16)–S(2)–Ni(1)	102.79(9)
Complex **3b**			
Ni(1)–S(1)	2.1292(8)	S(1)–Ni(1)–S(4)	86.94(3)
Ni(1)–S(2)	2.1340(9)	S(2)–Ni(1)–S(4)	179.02(4)
Ni(1)–S(3)	2.1354(8)	S(3)–Ni(1)–S(4)	92.59(3)
Ni(1)–S(4)	2.1371(9)	C(14)–S(1)–Ni(1)	103.23(9)
S(1)–Ni(1)–S(2)	92.45(3)	C(16)–S(2)–Ni(1)	103.61(10)
S(1)–Ni(1)—S(3)	179.42(4)	C(18)–S(3)–Ni(1)	103.08(9)
S(2)–Ni(1)–S(3)	88.02(3)	C(20)–S(4)–Ni(1)	103.26(10)
Complex **6**			
Pd(1)–S(1)	2.2762(14)	S(1A)–Pd(1)–S(1)	180.0
Pd(1)–S(2)	2.2909(14)	S(2A)–Pd(1)–S(2)	180.00(3)
S(1)–Pd(1)–S(2)	89.70(5)	C(14)–S(1)–Pd(1)	102.05(14)
S(1)–Pd(1)–S(2A)	90.30(5)	C(16)–S(2)–Pd(1)	101.77(15)

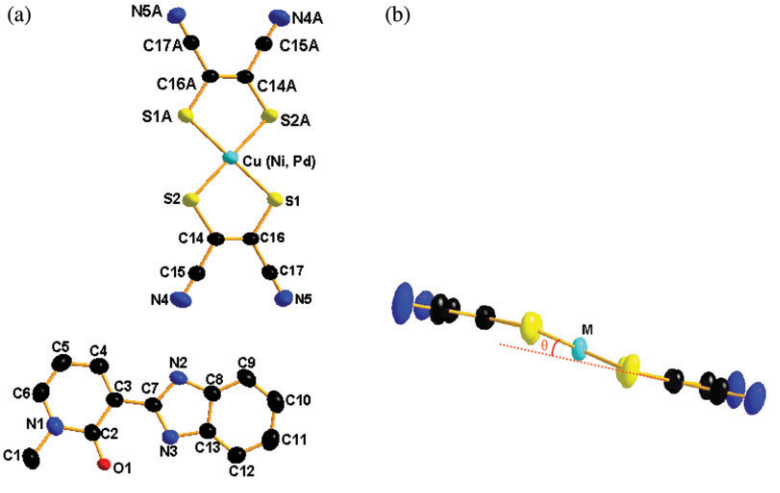

Figure 3. (a) ORTEP views of **2**, **3a**, and **6** with atom labeling and (b) Z-shaped nonplanar geometry (**2**, $\theta = 13.6°$; **3a**, $\theta = 10.2°$, and **6**, $\theta = 9.5°$) (hydrogen atoms are omitted for clarity).

parameters of $d_{N\cdots N} = 2.879(3)$ Å and $\angle N\text{–}H\cdots N = 160.9°$ for $N2\cdots N4$, $d_{N\cdots N} = 3.173(3)$ Å and $\angle N\text{–}H\cdots N = 123(2)°$ for $N3\cdots N5$ in **2**; $d_{N\cdots N} = 2.902(3)$ Å and $\angle N\text{–}H\cdots N = 161.3°$ for $N2\cdots N4$, $d_{N\cdots N} = 3.1781(38)$ Å and $\angle N\text{–}H\cdots N = 116°$ for $N3\cdots N5$ in **3**; $d_{N\cdots N} = 2.882(5)$ Å and $\angle N\text{–}H\cdots N = 160.7°$ for $N2\cdots N4$, $d_{N\cdots N} = 3.1793(68)$ Å and $\angle N\text{–}H\cdots N = 120.9°$ for $N3\cdots N5$ in **6**). There also exist similar intramolecular H-bonding interactions as found in **1** (figure 4b).

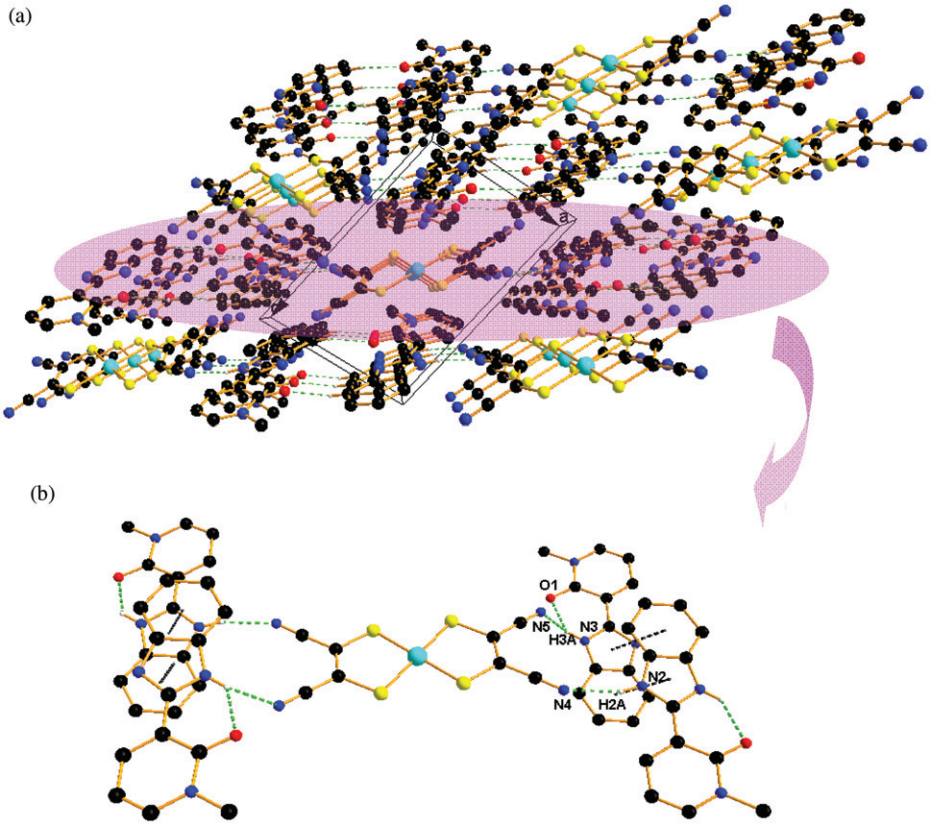

Figure 4. (a) The packing diagram of **2**, **3a**, and **6** as viewed along the *b*-axis showing the layered structure and (b) H-bonding interactions in layers.

Between neighboring molecular layers, there exist two intermolecular interactions. The $\pi\cdots\pi$ interactions are stronger between benzimidazole rings of neighboring layers (figure S2). The mode of these $\pi\cdots\pi$ interactions is offset face-to face. The centroid-to-centroid distances between imidazole ring and benzyl planes are 3.5974(6) Å in **2**, 3.6216(7) Å in **3a** and 3.6051(15) Å in **6**. The weaker interaction is anion$\cdots\pi$ interactions between the electron-deficient pyridinium ring of cation and the rich-electron MS_4 core of $[M(mnt)_2]^{2-}$ (figure S3). The distances between pyridyl ring and MS_4 plane are 3.7967(4) Å in **2**, 3.7747(5) Å in **3a**, and 3.8147(11) Å in **6**.

Compound **3b** crystallizes in the monoclinic space group $P2_1/n$. Because the stoichiometric ratio of cations and anions is 1 : 1, there are one $[Ni(mnt)_2]^-$ and one $[MOBIP]^+$ in an asymmetric unit (figure S4). The $[Ni(mnt)_2]^-$ exhibits a nearly planar geometry and the NiS_4 core exhibits a slightly distorted square-planar coordination geometry, different from **3a** (figure S5). As shown in table 3, the Ni–S bond distances of **3b** (2.1292(8) to 2.1371(9) Å) are unequal and shorter than those of **3a**. S–Ni–S bond angles are also smaller than those of **3a**, in agreement with the other reported $[Ni(mnt)_2]^-$ complexes [17, 20, 38].

The stacking columns of anions and cations for **3b** viewed along the *b*-axis are shown in figure 5. Similar to a reference [39], the anions (A) and cations (C) alternate to stack

Downloaded by [Renmin University of China] at 10:33 13 October 2013

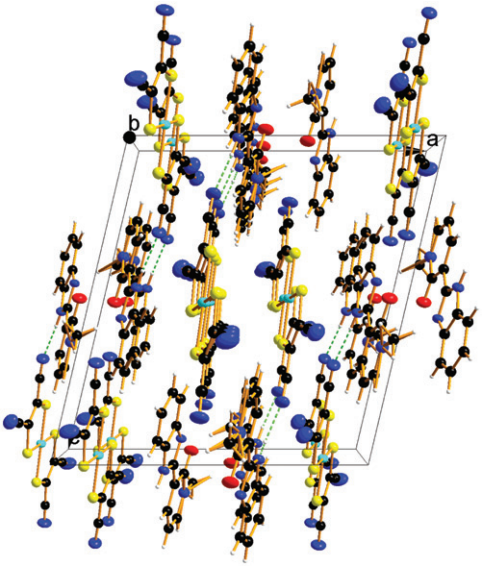

Figure 5. The packing diagram of **3b** as viewed along the *b*-axis.

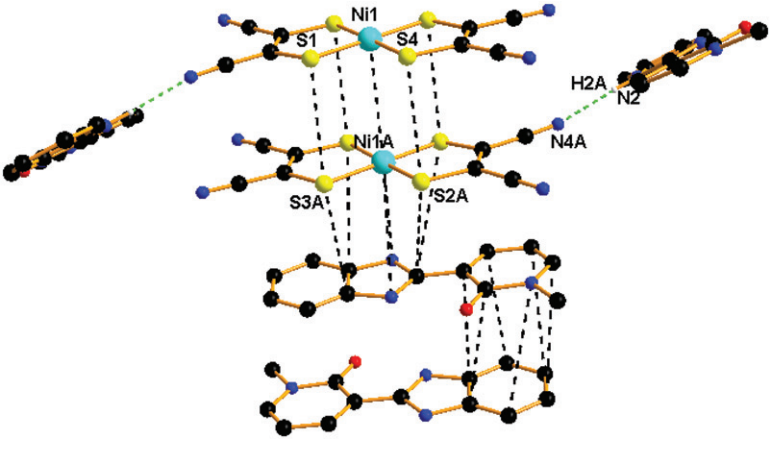

Figure 6. The intermolecular interactions in **3b** as viewed along the *a*-axis.

into a mixed 1-D column in the fashion of $\cdots$AACCAACC$\cdots$. In the column (figure 6), two neighboring $[Ni(mnt)_2]^-$ anions form a dimer *via* face-to-face stack with interatomic separations (3.7414 Å of Ni(1)$\cdots$Ni(1)^i, 3.7498 Å of S(1)$\cdots$S(3)^i, 3.7098 Å of S(2)$\cdots$S(4)^i, symmetric code $i = x, 1+y, -1+z$) owing to two $[Ni(mnt)_2]^-$ anions along the *a*-axis. The Ni$\cdots$Ni distance (3.7414 Å) between anions is smaller than that in the references. Two $[MOBIP]^+$ cations also form a dimer with an antiparallel arrangement, and the crystal packing of cations arises from medium strong π-stacking. The distance between pyridyl and phenyl rings is 3.7415(7) Å. Between neighboring $[Ni(mnt)_2]^-$ and $[MOBIP]^+$, there also exist anion$\cdots\pi$ interactions between the

Downloaded by [Renmin University of China] at 10:33 13 October 2013

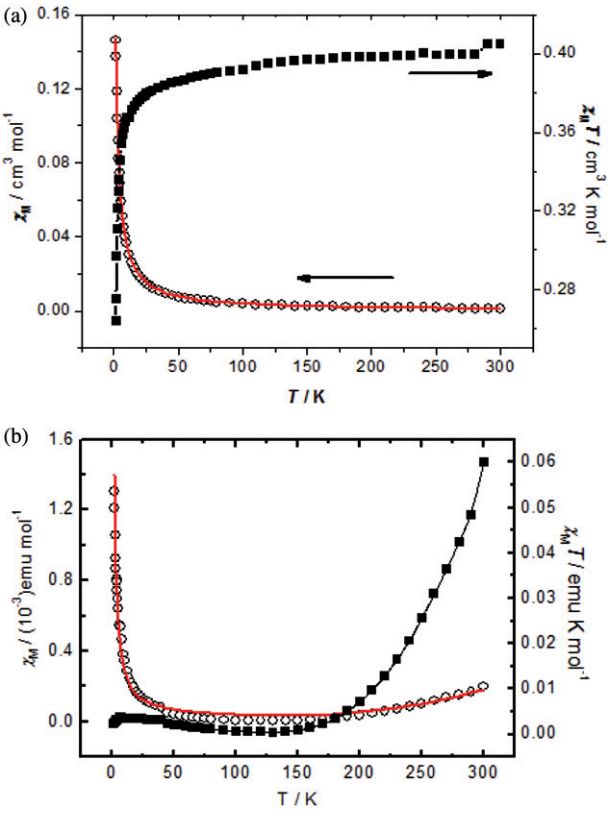

Figure 7. Temperature dependence of magnetic susceptibility in χ_m and $\chi_m T$ forms for **2** and **3b**.

electron-deficient pyridinium ring of cation and the rich-electron NiS_4 core of $[Ni(mnt)_2]^-$. The centroid-to-centroid distance between imidazoline ring and NiS_4 plane is 3.6734(8) Å.

As shown in figure 5, neighboring columns are connected *via* intermolecular H-bonding interactions between imidazoline of the cations and nitrile of the anions (with H-bonding parameters of $d_{N\ldots N} = 2.933(3)$ Å and $\angle N\text{–}H\cdots N = 175.9°$ for $N2\cdots N4$, $d_{N\ldots N} = 2.964(3)$ Å and $\angle N\text{–}H\cdots N = 140(2)°$ for $N3\cdots N6$) as well as van der Waals forces. The angle between the neighboring columns is 29.9°. These weak molecular interactions observed in **3b** result in formation of the 3-D supramolecular structure.

The difference of fluorescence spectra should be induced by the different intra- and inter-molecular interactions. Comparing structures of **2**, **3a**, **3b**, **6** with **1**, there exist similar intra- and inter-molecular H-bonding interactions. However, with iodide substituted by $[M(mnt)_2]^{n-}$, the π–π stacking interactions become weak and there exist new anion$\cdots\pi$ interactions between the electron-deficient pyridinium ring of cation and the rich-electron MS_4 core of $[M(mnt)_2]^{n-}$. Fluorescent quenching of these complexes is not mainly caused by the $\pi\cdots\pi$ stacking interactions among the cations but by the anion$\cdots\pi$ interactions.

Downloaded by [Renmin University of China] at 10:33 13 October 2013

Downloaded by [Renmin University of China] at 10:33 13 October 2013

3.5. *Magnetic properties*

Variable-temperature magnetic susceptibilities of **2** and **3b** have been investigated from 1.8 to 300 K. The diamagnetic correction was performed by Pascal's constants [40], and the magnetic susceptibility as χ_m and $\chi_m T$ are displayed in figure 7. As for **2** (figure 7a), the magnetic behavior exhibits weak antiferromagnetic coupling, and the value of $\chi_m T$ at 300 K is 0.405 emu K mol^{-1}, slightly larger than the value of 0.375 emu K mol^{-1} expected for a spin-only system with $S = ½$. The magnetic behavior can be interpreted in terms of the Curie–Weiss law (equation (1)):

$$\chi_m = C/(T - \theta). \tag{1}$$

Plots of the molar magnetic susceptibilities were fitted using equation (1) to give $\theta = -0.950$ K and $C = 0.406$ emu K mol^{-1}; the g value obtained from the Curie constant C is 2.08, which is very close to the average g value measured by EPR (2.04, figure S6). The small minus value of θ reveals antiferromagnetic interaction between adjacent Cu^{2+} ions is very weak, in agreement with the fact that there exist larger separations between neighboring magnetic anions (Cu $\cdots$ Cu distance = 8.632 Å).

For **3b** (figure 7b), the magnetic susceptibility data can be analyzed using simple dinuclear model approximation (the Hamiltonian being $H = -2J\ S_A S_B$) (equation (2) [41]):

$$\chi_m = (2N\beta^2 g^2/kT)(1 - \rho)/(3 + \exp(-2J/kT) + (N\beta^2 g^2/2kT)\rho + \chi_0, \tag{2}$$

where N, g, k, β, and ρ have their usual meanings [42] and J is the exchange coupling parameter describing the magnetic interaction between two neighboring $S = 1/2$ spins. The best fit parameters obtained by least-squares fit are $g = 2.14$, $J = -333.7$ cm^{-1}, $\rho = 1.49 \times 10^{-2}$, $\chi_0 = 1 \times 10^{-5}$ emu mol^{-1}, and $R = 3.44 \times 10^{-8}$ (R is defined as $\sum(\chi_m^{calcd} - \chi_m^{obsd})^2/\sum(\chi_m^{obsd})^2$). The negative value of J reveals the antiferromagnetic interaction between neighboring $[Ni(mnt)_2]^-$ anions and this is in agreement with the distance between two neighboring nickel anions (Ni $\cdots$ Ni distance = 3.741 Å), which is stronger than the antiferromagnetic interaction shown in the references. The model provides an excellent fit (the solid lines figure 7b), as indicated by the low value of R.

4. Conclusions

We obtained a new organic fluorescent ionic compound [MOBIP]I (**1**) by using 2-chloronicotinic acid instead of nicotinic acid to react with *o*-phenylenediamine. With substitution of the iodide by $[M(mnt)_2]^{n-}$ (M = Cu^{2+}, Ni^{2+}, Ni^{3+}, Zn^{2+}, Cd^{2+}, Pd^{2+}, and Pt^{2+}), seven maleonitriledithiolate metal complexes $[MOBIP]_n[M(mnt)_2]$ were prepared.

When these compounds were dissolved in DMF solution at room temperature, there is strong blue light fluorescence by irradiation of UV light. The quantum yields of fluorescent emission (ϕ_f) of these eight compounds are high at 0.45 to 0.70. These seven complexes in DMF are a new series of solution luminescent complexes of maleonitriledithiolate. They display similar symmetric emissions with λ_{em} at the deep blue region of ~426 nm upon excitation at ~364 nm in DMF, caused by **L**–**L** transition of $MOBIP^+$. This is different than previous solution luminescent maleonitriledithiolate

complexes. Existence of $[M(mnt)_2]^{n-}$ in the solution can prolong the fluorescent lifetimes; the maximum value of fluorescent lifetime in **7** is 3.92 ns, 0.16 ns longer than [MOBIP]I (**1**), while ϕ_f is still high at 0.67. The differences of these complexes' ϕ_f are caused by the influence on the photon transfer induced by $[M(mnt)_2]^{n-}$. Due to different shape and metal ionic radius of $[M(mnt)_2]^{n-}$, the ϕ_f decrease in the order $Pt^{2+} > Pd^{2+} > Ni^{2+} > Ni^{3+} > Cu^{2+} > Zn^{2+} > Cd^{2+}$.

For all of these compounds in the solid state, emission of **1** is blue-shifted and narrow compared to solution; fluorescence of the seven complexes is quenched. Based on their crystal structures, the $\pi\cdots\pi$ stacking interactions among cations in **1** and anion$\cdots\pi$ stacking interactions in complexes mainly cause the difference of their fluorescence spectrum.

Crystal analyses also reveal that **2**, **3a**, and **6** are isostructural and $[M(mnt)_2]^{2-}$ anions show rare Z-shaped nonplanar geometry, while **3b** crystallizes in the $P2_1/n$ space group and its anions (A) and cations (C) are stacked in a mixed column in the fashion of $\cdots$AACCAACC$\cdots$. Variable-temperature magnetic susceptibilities of **2** and **3b** reveal that **2** exhibits almost isolated spin system, while **3b** exhibits stronger antiferromagnetic coupling, because of the smaller Ni$\cdots$Ni distances in **3b** induced by the planar cation instead of the folded cation as the counter cation.

Downloaded by [Renmin University of China] at 10:33 13 October 2013

Supplementary material

CCDC 810779, 763560, 763561, 776708, and 776709 contains the supplementary crystallographic data of **1**, **2**, **3a**, **3b**, and **6** for this article. These data can be obtained free of charge from The Cambridge Crystallographic Data Centre *via* www.ccdc.cam.ac.uk/data_request/cif

Acknowledgments

This work was supported by the National Basic Research program of China (2007CB925102), the National Natural Science Foundation of China (NSFC: 20771056), the State Basic Research Project of China (NSFC: 20490218), and the Center of Analysis and Determining of Nanjing University.

References

[1] G.M. Cockrell, G. Zhang, D.G. VanDerveer, R.P. Thummel, R.D. Hancock. *J. Am. Chem. Soc.*, **130**, 1420 (2008).
[2] C.M.G. Dos Santos, T. McCabe, T. Gunnlaugsson. *Tetrahedron Lett.*, **48**, 3135 (2007).
[3] S.L. Oliveira, D.S. CorrTa, L. Misoguti, C.J.L. Constantino, R.F. Aroca, S.C. Zilio, C.R. Mendon. *Adv. Mater.*, **17**, 1890 (2005).
[4] F. He, L.L. Tian, X.Y. Tian, H. Xu, Y.H. Wang, W.J. Xie, M. Hanif, J.L. Xia, F.Z. Shen, B. Yang, F. Li, Y.G. Ma, Y.Q. Yang, J.C. Shen. *Adv. Funct. Mater.*, **17**, 1551 (2007).

[5] M. Albota, D. Beljonne, J.L. Bredas, J.E. Ehrlich, J.Y. Fu, A.A. Heikal, S.E. Hess, T. Kogej, M.D. Levin, S.R. Marder, D. McCord-Maughon, J.W. Perry, H. Rockel, M. Rumi, C. Subramaniam, W.W. Webb, X.L. Wu, C. Xu. *Science*, **281**, 1653 (1998).
[6] J. Kunzelman, M. Kinami, B.R. Crenshaw, J.D. Protasiewicz, C. Weder. *Adv. Mater*., **20**, 119 (2008).
[7] S.R. Forrest. *Nature*, **428**, 911 (2004).
[8] H. Langhals, O. Krotz, K. Polborn, P. Mayer. *Angew. Chem*., **117**, 2479 (2005).
[9] F. Gao, Q. Liao, Z.-Z. Xu, Y.-H. Yue, Q. Wang, H.-L. Zhang, H.-B. Fu. *Angew. Chem. Int. Ed*., **49**, 732 (2010).
[10] G. Accorsi, A. Listorti, K. Yoosaf, N. Armaroli. *Chem. Soc. Rev*., **38**, 1690 (2009).
[11] N. Armaroli, L.D. Cola, V. Balzani, J.-P. Sauvage, C. Dietrich-Buchecker, J.-M. Kern. *J. Chem. Soc., Faraday Trans*., **88**, 553 (1992).
[12] N. Robertson, L. Cronin. *Coord. Chem. Rev*., **227**, 93 (2002).
[13] T. Hisashi, O. Yoshinori, K. Hayao, S. Wakako, K. Akiko. *Science*, **291**, 285 (2001).
[14] T. Akutagawa, T. Nakamura. *Coord. Chem. Rev*., **226**, 3 (2002).
[15] A.E. Pullen, R.-K. Olk. *Coord. Chem. Rev*., **188**, 211 (1999).
[16] T. Akutagawa, T. Nakamura. *Coord. Chem. Rev*., **198**, 297 (2000).
[17] X.M. Ren, Q.J. Meng, Y. Song, C.S. Lu, C.J. Hu, X.Y. Chen. *Inorg. Chem*., **41**, 5686 (2002).
[18] Z.P. Ni, X.M. Ren, J. Ma, J.L. Xie, C.L. Ni, Z.D. Chen, Q.J. Meng. *J. Am. Chem. Soc*., **127**, 14330 (2005).
[19] Z.F. Tian, X.M. Ren, Y.Z. Li, Y. Song, Q.J. Meng. *Inorg. Chem*., **46**, 8102 (2007).
[20] H.B. Duan, X.M. Ren, Q.J. Meng. *Coord. Chem. Rev*., **254**, 1509 (2010).
[21] J.A. Zuleta, M.S. Burberry, R. Eisenberg. *Coord. Chem. Rev*., **97**, 47 (1990).
[22] J. Bremi, V. Gramlich, W. Caseri, P. Smith. *Inorg. Chim. Acta*, **322**, 23 (2001).
[23] G. Bahr, G. Schleitzer. *Chem. Ber*., **90**, 438 (1957).
[24] E. Alcalde, I. Dinares, J. Frigola, C. Jaime, J.P. Fayet, M.C. Vertut, C. Miravitlles, J. Rius. *J. Org. Chem*., **56**, 4223 (1991).
[25] C. Marzin, M.E. Peek, J. Elguero, H.P. Figeya, N. Defay. *Heterocycles*, **6**, 911 (1977).
[26] *Software packages SMART and SAINT*, Bruker AXS Inc., Madison, WI (2000).
[27] G.M. Sheldrick. *SHELXL-97, Program for the Refinement of Crystal Structure*, University of Göttingen, Germany (1997).
[28] E. Ribera, C. Rovira, J. Veciana, J. Tarres, E. Canadell, R. Rousseau, E. Molins, M. Mas, J.-P. Schoeffel, J.-P. Pouget, J. Morgado, R.T. Henriques, M. Almeida. *Chem. Eur. J*., **5**, 2205 (1999).
[29] A. Gilbert, J. Baggott. *Essentials of Molecular Photochemistry*, Blackwell Scientific Publications, Oxford, UK (1991).
[30] J.A. Zuleta, J.M. Bevilacqua, D.M. Proserpio, P.D. Harvey, R. Eisenberg. *Inorg. Chem*., **31**, 575 (1992).
[31] A.T.R. Williams, S.A. Winfield, J.N. Miller. *Analyst*, **108**, 1067 (1983).
[32] H. Kisch, B. Eisen, R. Dinnebier, K. Shankland, W.I.F. David, F. Knoch. *Chem. Eur. J*., **7**, 738 (2001).
[33] K.S. Siddiqi, S. Bano, A. Mohd, A.A.P. Khan. *Chin. J. Chem*., **27**, 1755 (2009).
[34] Y. Wang, L. Yi, B. Ding, P. Cheng, D.-Z. Liao, S.-P. Yan. *Inorg. Chem*., **45**, 5822 (2006).
[35] L.-F. Yang, Z.-H. Peng, G.-Z. Cheng, S.-M. Peng. *Polyhedron*, **22**, 3547 (2003).
[36] M. Egli, S. Sarkhel. *Acc. Chem. Res*., **40**, 197 (2007).
[37] C.Q. Wan, X.D. Chen, T.C.W. Mak. *CrystEngComm*., **10**, 475 (2008).
[38] C.-L. Ni, Q. Huang, H.-R. Zuo, Y. Hou, Q.-J. Mang. *J. Coord. Chem*., **62**, 1502 (2009).
[39] H.B. Duan, H. Zhou, Z.F. Tian, F. Xuan, X.M. Ren. *Solid State Sci*., **11**, 1216 (2009).
[40] S. Alvarez, R. Vicente, R. Hoffmann. *J. Am. Chem. Soc*., **107**, 6253 (1985).
[41] X.M. Ren, T. Akutagawa, S. Nishihara, T. Nakamura. *Synth. Met*., **150**, 57 (2005).
[42] Y. Song, D.R. Zhu, K.L. Zhang, Y. Xu, C.Y. Duan, X.Z. You. *Polyhedron*, **19**, 1461 (2000).

Downloaded by [Renmin University of China] at 10:33 13 October 2013